Water Practice & Technology

IWA PUBLISHING

Water Practice & Technology Vol 18 No 9, 2193 doi: 10.2166/wpt.2023.126

Rice husk charcoal and acid modified rice husk charcoal for efficient adsorption of methyl orange

Samina Zaman[a,*], Mst. Kaniz Fatema[a], Sujoy Sen[a], Rafiuz Zaman[b], Tapos Kumar Chakraborty[a], Nishat Tasnime[a], Monirul Islam[a], Sangina Haque[a], Ahsan Habib[a] and Gopal Chandra Ghosh[a]

[a] Department of Environmental Science and Technology, Jashore University of Science and Technology, Jashore, Bangladesh
[b] School of Organisations, Systems and People, Faculty of Business and Law, University of Portsmouth, Portsmouth, UK
*Corresponding author. E-mail: samina@just.edu.bd

ABSTRACT

In this study, methyl orange (MO) was removed from solution using rice husk charcoal (RHC) and acid modified rice husk charcoal (AMRHC). In batch adsorption mode, contact time (1–240 min), pH (3–10), adsorbent dose (1–30 g/L), and initial MO concentration (10–100 mg/L) were investigated. Fourier transform infrared spectroscopy (FTIR) and scanning electron microscopy (SEM) were used to characterize the adsorbent's surface morphology and chemistry. At equilibrium, the highest removal of MO by RHC and AMRHC were 89 and 99%, respectively. Removal efficiency increased with increasing adsorbent dose, while the opposite was observed for adsorption capacity because of the availability of unsaturated adsorption sites. RHC and AMRHC were best described by the Freundlich and Langmuir isotherm models, with maximum adsorption capacities of 4.57 and 11.53 mg/g, respectively. The pseudo-second-order kinetic model fitted well for both adsorption and chemisorption, and the process was controlled by multi-step diffusion. Thermodynamic measurements proved that dye adsorption is a spontaneous endothermic process.

Key words: acid modified rice husk charcoal, adsorption, isotherms, kinetics, methyl orange, rice husk charcoal

HIGHLIGHTS

- MO adsorption was studied using RHC and AMRHC.
- About 89 and 99% of MO dye were removed by RHC and AMRHC, respectively.
- The maximum adsorption capacities were 4.57 and 11.53 mg/g, for RHC and AMRHC, respectively.
- Kinetic data followed pseudo-second-order kinetics for both adsorbents.
- The adsorption potential of both adsorbents for the treatment of MO dye was compared with other adsorbents which is cost effective.

INTRODUCTION

Globally, industrial and urban developments are tremendously increasing due to rising population growth, which significantly enhances environmental pollution (Carolin *et al.* 2021). Diverse industrial activities release large amounts of wastewater, which finally goes to the aquatic and terrestrial environments, which is a matter of serious concern (Radoor *et al.* 2021). Dyes are widely used in many industries and discharged as colored effluent in aqueous environments where they can cause many difficulties, including reduction of the rate of photosynthesis, hindering sunlight penetration, chelating metal ions, and generating diseases for aquatic flora and fauna (Carolin *et al.* 2021; Zaman *et al.* 2021). Additionally, dyes can create human health hazards, such as skin and eye problems, and diarrhea, and act as mutagenic and carcinogenic agents (Chakraborty *et al.* 2021). Depending on their chemical structure, there are three dye types: cationic, anionic, and nonionic. MO is an anionic azo-dye that is commonly used as a coloring agent (Radoor *et al.* 2021), the textile industry alone producing 7×10^5 tonnes/year of toxic dyes and associated byproducts (Kubendiran *et al.* 2021). Though different physicochemical properties of MO including lower degradation rate, aromatic ring structure, and high retaining capacity make it difficult to remove from effluents but it must be free from effluents before discharges into the receiving environment.

Different treatment technologies including oxidation, membrane filtration, reverse osmosis, coagulation and flocculation, ion exchange, adsorption, nanofiltration, ultrafiltration, etc., have been used to remove toxic dyes from effluent (Bensalah *et al.* 2020), where adsorption is superior to other techniques in terms of cost-effectiveness, ease of operation, energy input, and low probability of further byproduct formation (Zaman *et al.* 2021). High production costs reduce the use of commercial activated carbon as an adsorbent material. Furthermore, researchers are trying to produce cost-effective alternative adsorbents from biomaterials such as solid waste products, natural discard materials, and agro-processing byproducts (Ghosh *et al.* 2020; Zaman *et al.* 2021), including cotton waste, sawdust, silica gel, bark, rice husk, natural coal, peat, chitosan, jute stick, activated carbon, activated clay, and hen feathers (Chakraborty *et al.* 2020; Zaman *et al.* 2021).

Recently, agro-processing byproducts (e.g., rice husks) have received consideration due to their ready availability, low or zero cost, and natural properties (Leng *et al.* 2015). They also contain high proportions of cellulose (55–65%), SiO_2 (15–20%), and 20% lignin (Fu *et al.* 2019). Rice husk has no good nutritional status and is rarely used as cattle food, but is used as cooking, paving, and landfilling materials.

Rice husk charcoal (RHC) was produced by burning rice husks, and acid modified rice husk charcoal (AMRHC) was formed by treating RHC with acid to increase the sorption capacity. RHC was used as an adsorbent for textile effluent treatment in this study. The objectives were (i) to assess the performance of RHC and AMRHC for MO dye removal from simulated wastewater with diverse experimental conditions (pH, adsorbent dose, contact time, and initial dye concentration) and (ii) to estimate the adsorption actions of RHC and AMRHC using adsorption kinetics and isotherms.

MATERIALS AND METHODS

Adsorbent preparation

Preparation of RHC

Rice husk was collected in Chougacha, Jashore, soaked in distilled water for 1.5 h, and washed with distilled water numerous times. It was then dried in an oven (Labtech LDO-150F, Korea) for 48 h at 80 °C, and then in a muffle furnace (SXT-10, Shanghai Shuli Instrument and Meters Co., Ltd, China) for carbonization at 400 °C for 10 min. The charcoal was pulverized using a mortar and pestle, and sieved to get the 0.1–0.5 mm-sized particles. The charcoal was kept in a sealed, borosilicate glass bottle for further use.

Preparation of AMRHC

The rice husk was washed and dried in the oven, before a grinder was used to grind and sieve it to get the 0.1–0.5 mm material. Next, 50 g of the material were mixed with 50 mL of concentrated (18M) H_2SO_4 (impregnation ratio = 1:1) and stored for 12 h at room temperature. After 12 h, it was heated to 70 °C for 1.5 h using a hot plate, then diluted with distilled water numerous times until the pH was 7, and finally left for 24 h in an oven at 80 °C and stored in a borosilicate glass bottle.

Chemicals and instrumentation

MO dye was acquired from Sigma-Aldrich, USA. The molecular weight of MO is 327.34 g/mol, its chemical structure $C_{14}H_{14}N_3NaO_3S$, pH range 3–4.4, and purity, in this case, 85%. This adsorbate was used as-received. All chemicals used were analytical grade. The required amount of MO was dissolved in double-distilled water to prepare the MO stock solution (400 mg/L) from which the desired working solution was prepared. The experimental pH was adjusted using a 0.1 N HCl/0.1 N NaOH solution, and determined with a pH meter (Ezdo 6011, Taiwan). A UV-visible spectrophotometer (HACH DR 3900, USA) was used to measure the MO concentration in the solution at 464 nm wavelength.

Adsorption experiments

The stock solution (1,000 mg/L) of MO was prepared by dissolving the required quantity of dye powder in double-distilled water and keeping the stock solution's pH at 3.0 using HCl. Successive dilutions were used to prepare the working solution from the stock solution. MO adsorption onto RHC and AMRHC was observed in batch experiments, stirred at 180 rpm, and its dependence on contact time (1–240 min), pH (pH 3–10), adsorbent dose (1–30 g/L), and initial dye concentration (10–100 mg/L). For pH adjustment, a 0.1 N acid (HCl) and base (NaOH) solution was used. The working solution for the experiments was 250 mL in a 500 mL beaker stirred in a jar-tester (JLT4, VELP Scientifics, Italy). Each experiment was completed with a suitable amount of

suspension removed from the beaker and filtered to eliminate adsorbent particles using a glass microfiber filter paper (GF/B, Whatman, USA). The concentration of MO in the solutions before and after treatment was measured. A duplicate test was conducted to ensure accurate results. Equations (1) and (2) were used to calculate the amount of MO adsorption at equilibrium and removal (%), respectively:

$$q_e = \frac{(C_0 - C_e)V}{m} \tag{1}$$

$$R\ (\%) = \frac{(C_0 - C_e)}{C_0} \times 100 \tag{2}$$

where C_0 is the initial dye concentration (mg/L); C_e is the equilibrium concentrations (mg/L); q_e is the equilibrium MO adsorbed (mg/g); V is the solution volume (L); and m is the adsorbent mass (g).

MO isotherm experiments

The adsorption isotherm tests were conducted using 250 mL of MO solutions in several 500 mL beakers at diverse MO concentrations ranging from 10 to 100 mg/L, with the following common experimental conditions: RHC and AMRHC dose (10 g/L), rotation speed (180 rpm), pH (3), temperature (25 °C), and contact time (150 min). Adsorption isotherms deliver a complete knowledge of the types of associations by demonstrating how the adsorbate behaves with sorbent materials. In this study, the Langmuir, Freundlich, Elovich, and Halsey isotherm models were used, as detailed in Supplementary Table S1.

MO adsorption kinetic experiments

The adsorption kinetic studies involved adding 10 g/L charcoal to a 350 mL solution, which had 20 mg-MO/L at pH 3 and was agitated at 180 rpm at 25 °C. At specific times – 1, 2, 3, 5, 7, 10, 30, 60, 90, 120, 150, 180, 210, and 240 – samples were taken from the solution, filtered, and analyzed. Adsorption kinetics includes details of the rate of MO adsorption by the adsorbents, the amount of time needed to complete the process, and the reaction mechanism. The kinetic behavior was identified using Ho and McKay's pseudo-second-order model and Lagergren's pseudo-first-order model, whereas the intraparticle diffusion model and Boyd model were employed to observe the possible adsorption process rate-controlling step and diffusion mechanism, as detailed in Supplementary Table S1.

Adsorption thermodynamics

Using optimum conditions, adsorption thermodynamics tests were carried out at 25, 40, 50, and 60 °C. Equations (3)–(5) were used to compute the thermodynamic parameters: K_d, ΔG (kJ mol^{-1}), R (8.314 J mol^{-1} K^{-1}), T (K), and ΔH (kJ mol^{-1}) defined, respectively, as the equilibrium partition constant, Gibbs free energy change, universal gas constant, experimental temperature, and enthalpy change (Yönten *et al.* 2020):

$$K_d = \frac{q_e}{c_e} \tag{3}$$

$$\Delta G = -RT \ln K_d \tag{4}$$

$$\ln K_d = \frac{\Delta S}{R} - \frac{\Delta H}{RT} \tag{5}$$

The values of ΔH and ΔS were determined from the slope and intercept of the plot of ln K_d versus $1/T$, respectively, and the values of ΔG from the K_d value at each temperature.

Desorption study

MO-loaded RHC and AMRHC were obtained from equilibrium adsorption studies for the desorption analysis. The adsorbents were subsequently filtered and dried for 24 h at 80 °C in the oven. Adsorbent loaded with MO dye was added to pH-controlled distilled water (pH 5, 7, 9, and 11) for 150 min at a continuous rotating speed of 180 rpm. Equation (6) was used to compute the proportional desorption from the amount of MO desorbed:

$$\text{Desorption}\ (\%) = \frac{\text{Mass of dye desorbed(mg/L)}}{\text{Mass of dye adsorbed(mg/L)}} \times 100 \tag{6}$$

RESULTS AND DISCUSSION

Adsorbent characterization

FTIR was used to identify the functional groups in the adsorption material. Figure 1 presents the FTIR spectra of both RHC and AMRHC. Peaks at 3,445, 1,616, and 1,094 cm^{-1} were present in the RHC spectrum, which is shown in green. The existence of both free and hydrogen bond OH groups was determined by the peak position at 3,445 cm^{-1}. The primitive peaks of RHC were 1,616 cm^{-1} (C = C stretching vibration) and 1,094 cm^{-1} (C–O stretching vibration). The yellow curve represents the MO-loaded RHC spectrum, where hydroxyl and carboxyl groups, C–O stretching vibration, and C–C skeleton vibration are represented at 3,451, 1,615, 1,101, and 469 cm^{-1}, respectively. Arumugam *et al.* (2018) found comparable results where rice husk carbon was applied for rhodamine B removal. The FTIR spectra of AMRHC in sky-blue and purple showed strong peaks at 3,418, 2,360, 1,621, and 1,113 cm^{-1} (–OH, N–H, C = C, and C–O, respectively), and shifted to 3,419, 2,362, 1,699, and 1,107, respectively, after binding with MO. Palapa *et al.* (2020) found similar types of peaks for the removal of cationic dye by CuAl LDH/rice husk biochar composite.

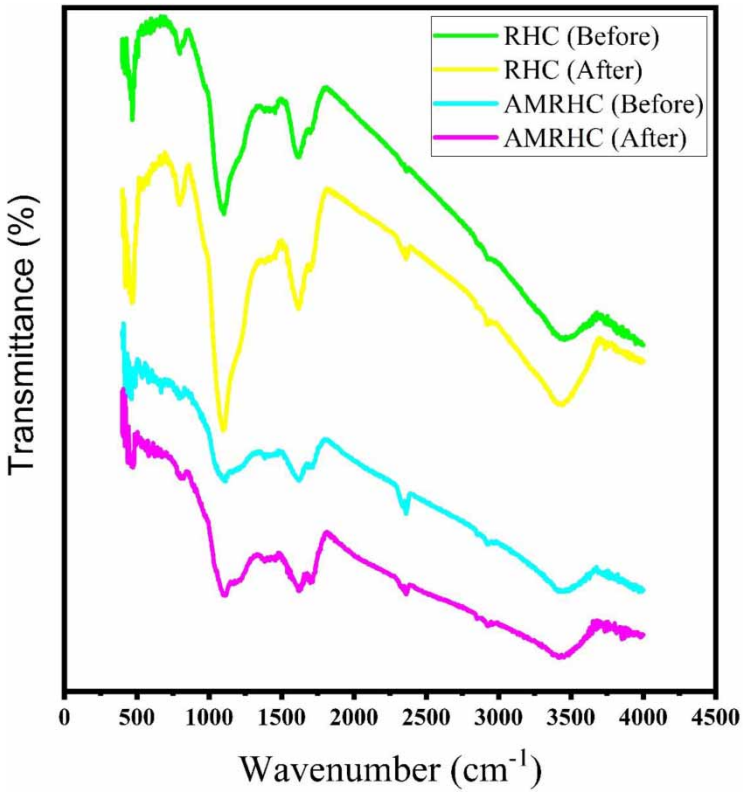

Figure 1 | FTIR spectra of (a) RHC before, (b) RHC after and (c) AMRHC before, (d) AMRHC after adsorption of MO. Please refer to the online version of this paper to see this figure in colour: https://dx.doi.org/10.2166/wpt.2023.126.

Energy-dispersive spectroscopy EDS and scanning electron microscopy (SEM) were both used to characterize the sorbents (RHC and AMRHC). The SEM images of RHC and AMRHC before (Figure 2(a) and 2(d)) adsorption of MO showed the particle morphologies and confirmed that the prepared adsorbents are irregular and porous, respectively. In the SEM image of RHC and AMRHC after (Figure 2(c) and 2(f)) adsorption of MO, the surfaces were becoming smooth because MO molecules were bound to the adsorbent's surface. The fresh RHC and AMRHC adsorbent surfaces contain significant amounts of elements C, N, O, and Si (Figure 2(b) and 2(e)). Ghosh *et al.* (2018) found a similar type of observation where they used rice husk and rice husk ash.

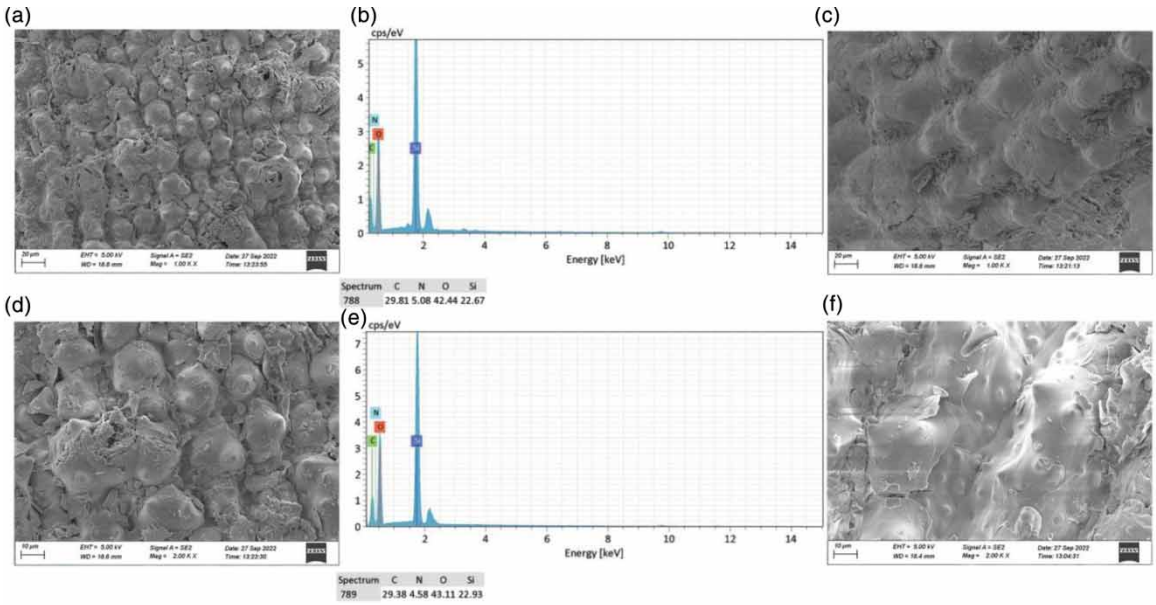

Figure 2 | SEM and EDS photographs of RHC (a, before adsorption; b, EDS of unloaded RHC; c, after adsorption) and AMRHC (d, before adsorption; e, EDS of unloaded AMRHC; f, after adsorption) adsorption of MO.

Effect of contact time and pH

Effect of contact time

The effect of contact time on MO dye adsorption using both adsorbents was carried out under standard conditions – pH = 3, adsorbent dose = 10 g/L, temperature = 25 °C, and rotation speed = 180 rpm. Samples were taken at designated times (see above). The results are presented in Figure 3(a). MO removal efficiency and adsorption capacity improved for both RHC and AMRHC with increasing time. In the first 30 min, the adsorption process changed rapidly due to the ready availability of vacant sites. After that, it changed slowly because of the lower driving force and fewer vacant spaces. The equilibrium state is achieved at 150 min for RHC and 120 min for AMRHC (Figure 3(a)). For this reason, all batch experiments were conducted at 150 min for RHC and 120 min for AMRHC. Lafi & Hafiane (2016) found a similar type of study for MO removal onto modified coffee waste.

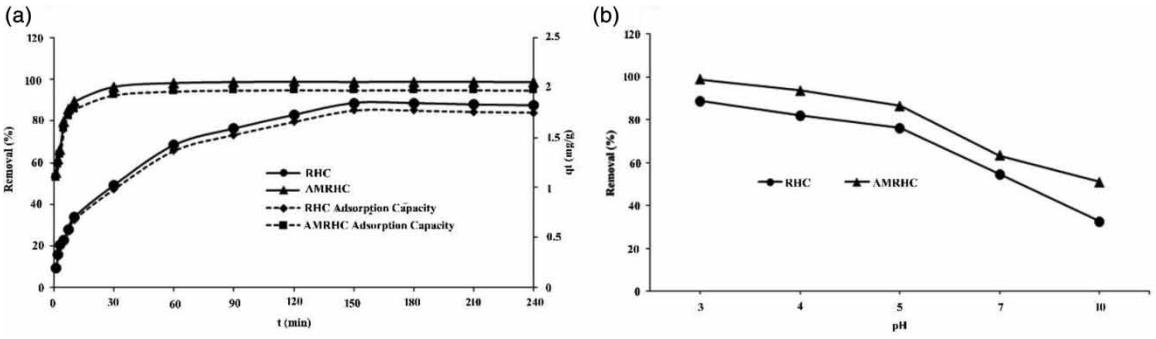

Figure 3 | Effect of (a) contact time and (b) pH on removal of MO by RHC.

Effect of pH

In the adsorption study, pH is considered dynamic because it affects the dye ionization rate, alters adsorbent inner and outer binding sites, and changes the adsorbent surface (Alardhi *et al.* 2023). Figure 3(b) displays the adsorption performance of MO dye using RHC and AMRHC in diverse solutions ranging in pH from 3 to 10. The MO removal efficiency for RHC (89–33%) and AMRHC (99–51%) and adsorption rate for RHC (1.77–0.65 mg/g) and AMRHC (1.98–1.02 mg/g) fell progressively with rising pH, and the best removal being was

found at pH 3 (Figure 3(b)). In acidic solution, MO's sulfonate group is dissociated and transformed into anionic colors, and electrostatic interaction increases between adsorbent and adsorbate – see Equations (7) and (8):

$$R - SO_3Na + H_2O \leftrightarrow R - SO_3^- + Na^+ \quad (7)$$

The highest removal efficiency arises from strong electrostatic interaction between anionic dye molecules and a positively charged adsorbent surface.

$$(R - SO_3^- + N^+) + \text{adsorbent (RHC and AMRHC) surface} \leftrightarrow \text{Adsorption of MO} \quad (8)$$

Huang *et al.* (2017) proposed a similar type of clarification for MO removal using protonated, cross-linked chitosan. Conversely, in a basic environment, the electrostatic repulsion between the MO ion and the adsorbent surface charge reduces the adsorption performance of RHC and AMRHC.

Effects of adsorbent dose

Adsorbent dose, a crucial factor that affects impurity removal from effluent, can be used to evaluate the adsorbate's adsorption capability (Zaman *et al.* 2022). To assess the appropriate dose, batch adsorption tests of MO onto RHC and AMRHC were conducted at 25 °C with diverse doses (1–30 g/L) but the other conditions constant (as above). The proportional MO removal onto RHC and AMRHC improved from 37 to 96% and 68 to 99% with the rising doses (Figure 4(a)), respectively, due to the additional active adsorbent surface sites. Former experiments achieved similar types of reports by converting industrial waste phosphogypsum into hydroxyapatite nanorods for removal of congo red (Bensalah *et al.* 2020). The proportional MO adsorption capacity fell slowly from 7.46 to 0.64 mg/g for RHC and 13.61 to 0.66 mg/g for AMRHC, with increasing adsorbent dose, possibly because of the saturation of most adsorption sites at high doses of adsorbent. A similar result has been reported for MO dye adsorption using Mahagoni bark charcoal (Ghosh *et al.* 2020).

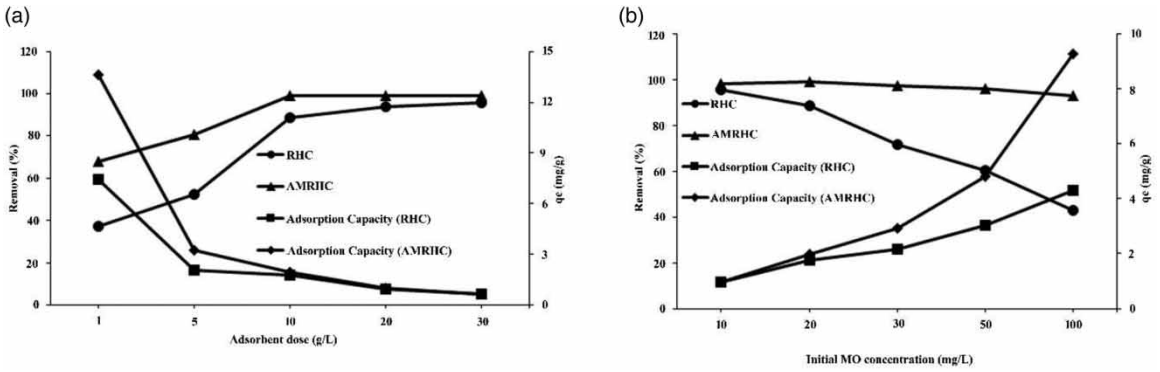

Figure 4 | Effect of (a) adsorbent dose and (b) initial MO concentration on removal of MO by RHC and AMRHC.

Effects of initial MO concentration

Figure 4(b) shows that the MO removal rate decreases (96–43% for RHC and 98–93% for AMRHC) as the initial MO dye concentration increases from 10 to 100 mg/L, because, at any fixed dose, the adsorbent's outer layer is covered by dye molecules. While the adsorption rate of MO gradually rises (0.96–4.29 mg/g for RHC and 0.98–9.29 mg/g for AMRHC) with rising MO concentration (10–100 mg/L) at constant RHC and AMRHC dose (10 g/L) (Figure 4(b)), the higher association between MO molecules and adsorbent (RHC and AMRHC) improved the major dynamic to shift a greater mass of MO from the liquid to the solid phase in an aqueous environment (Huang *et al.* 2017).

Adsorption isotherms

The association between adsorbate and adsorbent is described by adsorption isotherms (Zaman *et al.* 2021), and the Langmuir, Freundlich, Elovich, and Halsey isotherms were used in this study (Figures 5 and 6 and Table 1).

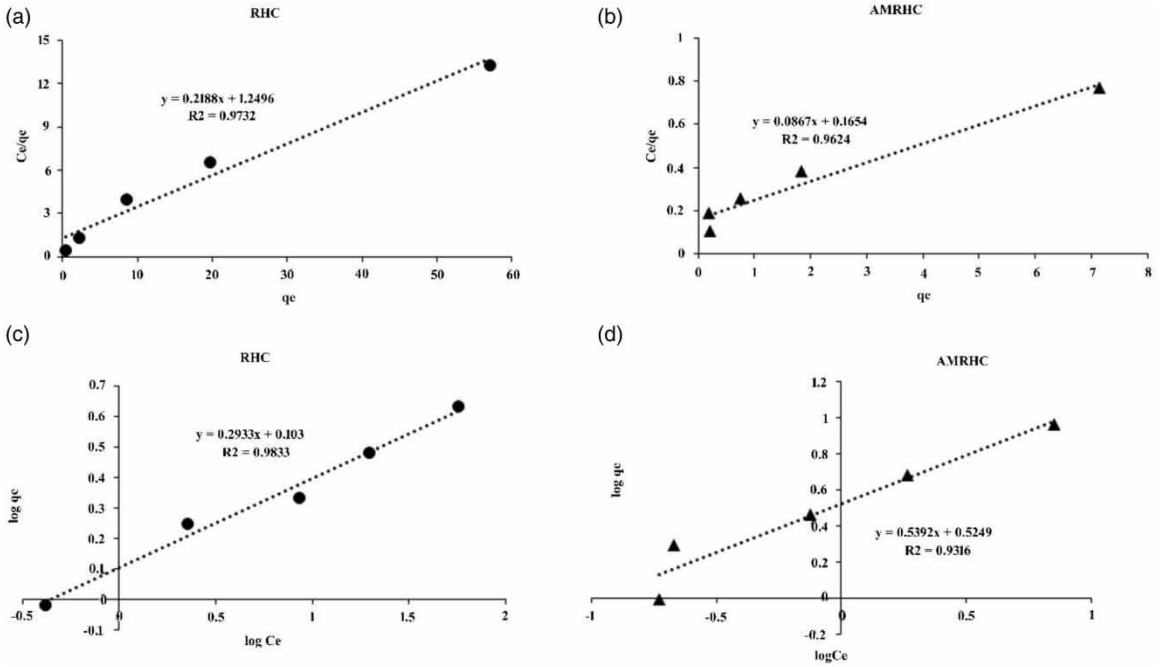

Figure 5 | MO adsorption isotherms onto RHC ((a) Langmuir and (c) Freundlich) and AMRHC ((b) Langmuir and (d) Freundlich).

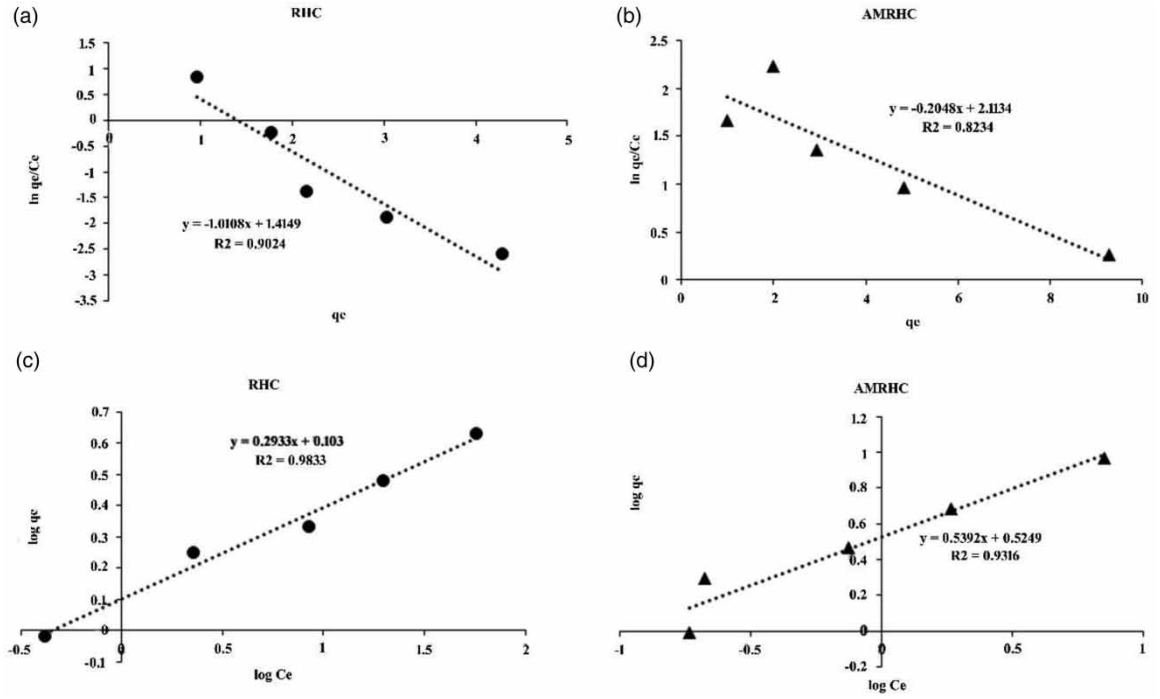

Figure 6 | MO adsorption isotherms onto RHC ((a) Elovich and (c) Halsey) and AMRHC ((b) Elovich and (d) Halsey).

Freundlich and Halsey were the best-fits for MO adsorption onto RHC ($R^2 = 0.983$ and 0.983, respectively). R^2 for Langmuir and Elovich, respectively, was 0.973 and 0.902. AMRHC, however, followed Langmuir ($R^2 = 0.962$) rather, than Freundlich ($R^2 = 0.932$), Elovich (0.823), or Halsey (0.932) (Table 1), suggesting that MO molecules produce multilayers on RHC and a single continuous layer on AMRHC. The monolayer maximum adsorption capacities of MO onto RHC and AMRHC were 4.57 and 11.53 mg/g (Table 1), respectively. The dimensionless constant separation factor R_L values of RHC (0.364–0.054) and AMRHC (0.16–0.019) were between 0 and 1,

Table 1 | Isotherm parameters for MO adsorption on RHC and AMRHC

Model	Parameter	Values (RHC)	Values (AMRHC)
Langmuir	q_{max} (mg/g)	4.57	11.53
	b (L/mg)	0.18	0.52
	R_L	0.364–0.054	0.16–0.019
	R^2	0.973	0.962
Freundlich	K_f (mg/g)	1.268	3.349
	N	3.409	1.855
	R^2	0.983	0.932
Elovich	q_m (mg/g)	0.989	4.882
	K_e	4.179	1.542
	R^2	0.902	0.823
Halsey	n_H	3.409	1.855
	K_H	2.245	9.408
	R^2	0.983	0.932

indicating that the experimental conditions were appropriate for MO adsorption onto RHC and AMRHC. Conversely, the adsorption intensity (n) ($n = 3.409$ for RHC and $n = 1.855$ for AMRHC) exceeded 1, and was higher than K_f (=1.268 for RHC and 3.349 for AMRHC), demonstrating that adsorption was promising for MO from aqueous solutions using both adsorbents (Table 1). Additionally, the performance of MO dye adsorption using RHC and AMRHC is comparable with other adsorbents, as presented in Supplementary Table S2.

Adsorption kinetics

Lagergren's pseudo-first-order and Ho and McKay's pseudo-second-order kinetic models were used in this study (Figure 7(a) and 7(b)). Model accuracy is measured by its correlation coefficient (R^2). The model parameters used are shown in Table 2. The pseudo-second-order kinetic model shows higher R^2 for MO adsorption than the pseudo-first-order model, for both adsorbents. The calculated adsorption capacity values for ($q_{e,cal}$ – 1.887 for RHC and 1.988 for AMRHC) the pseudo-second-order kinetic model equation also correspond to the experimental values (1.775 for RHC and 1.979 for AMRHC), indicating that the pseudo-second-order was the best-fit for the

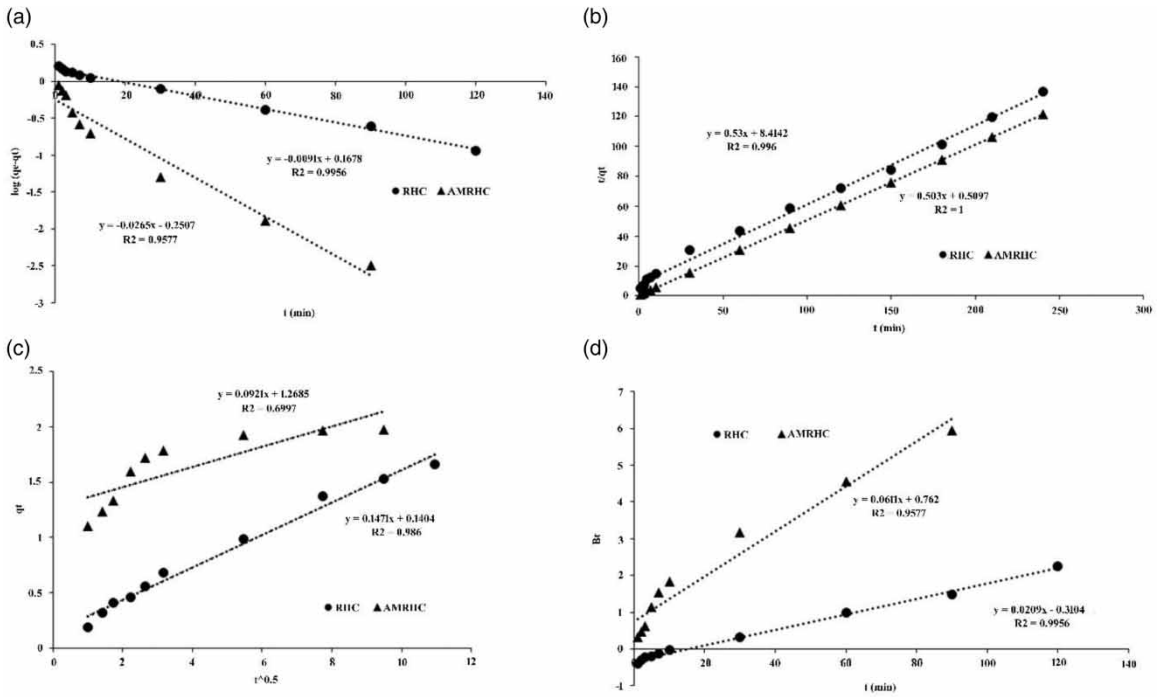

Figure 7 | MO kinetic adsorption on RHC and AMRHC using: (a) the pseudo-first-order, (b) pseudo-second-order, (c) intraparticle diffusion, and (d) Boyd kinetic models.

Table 2 | Kinetic parameters for MO adsorption onto RHC and AMRHC

Model	Parameter	Values (RHC)	Values (AMRHC)
Pseudo-first-order	$q_{e,\exp}$ (mg/g)	1.775	1.979
	q_e (mg/g)	1.472	0.003
	K_1	0.021	0.061
	R^2	0.996	0.958
Pseudo-second-order	$q_{e,\exp}$ (mg/g)	1.775	1.979
	q_e (mg/g)	1.887	1.988
	K_2	0.033	0.496
	h (mg/g/min)	0.119	1.962
	R^2	0.996	1
Intraparticle diffusion	K_{id} (mg/g/min$^{0.5}$)	0.147	0.092
	C	0.14	1.269
	R^2	0.986	0.7
Boyd	R^2	0.996	0.958

adsorption data, and showing that chemisorption involving electron sharing or exchange among MO and RHC was an adsorption process (Zaman *et al.* 2021).

To identify the diffusion mechanism, the interparticle diffusion (IP) model is used in this study. The IP plot did not pass through the origin (Figure 7(c)), and had high intercept values ($C = 0.14$ for RHC and 1.269 for AMRHC) (Table 2), indicating that the diffusion might be external and film site of the adsorbent (Chakraborty *et al.* 2021). While the Boyd plot showed (Figure 7(d)) that film diffusion was the rate-controlling step for MO adsorption onto RHC and AMRHC.

Adsorption thermodynamics studies

The parameters studied thermodynamically are presented in Table 3. A plot of ln K_d versus $1/T$ using Equations (3)–(5) yielded a straight line, with $R^2 = 0.909$ for RHC and 0.869 for AMRHC. When the solution temperature rises, the proportional removal increases, as shown in Figure 8(a), indicating that an endothermic process is involved during adsorption, and suggesting that MO's apparent adsorption mechanism onto both RHC and AMRHC is primarily a chemisorption process, in the presence of a weak link between the adsorbate and adsorbent. The negative value of ΔG^0 indicates that the adsorption process was spontaneous (Umpuch & Sakaew 2013), while the positive value of ΔH^0 confirms the endothermic nature of the adsorption process, indicating that dye uptake increases with increasing temperature, as supported by Figure 8(a). The positive value of ΔS^0 also suggests an increase in randomness in the adsorbent and MO molecule interface, caused mainly by the chemisorption mechanism through the ion exchange process (Umpuch & Sakaew 2013).

Table 3 | Thermodynamic parameters of MO adsorption onto RHC and AMRHC at different temperatures

	RHC				AMRHC			
Temperature (K)	ΔG^0 (kJ mol^{-1})	ΔS^0 (J mol^{-1} K^{-1})	ΔH^0 (kJ mol^{-1})	R^2	ΔG^0 (kJ mol^{-1})	ΔS^0 (J mol^{-1} K^{-1})	ΔH^0 (kJ mol^{-1})	R^2
298	0.592	119.771	36.683	0.909	−5.519	45.122	8.024	0.869
313	−0.031				−5.972			
323	−2.017				−6.422			
333	−3.566				−7.161			

Desorption study

Desorption is applied to assess the possibility of further contamination when the treated adsorbent enters the environment. The process is wholly controlled by chemical bonding (ionic, covalent, Van der Waals' forces, or dipole–dipole interaction) between adsorbent and adsorbate (Chakraborty *et al.* 2021). In this study, desorption was studied at pH values from 4 to 10. Figure 8(b) shows that the proportional desorption from RHC (13–19%) and AMRHC (21–38%) was low; instead of increasing pH, might be the strong and weak chemical bonding

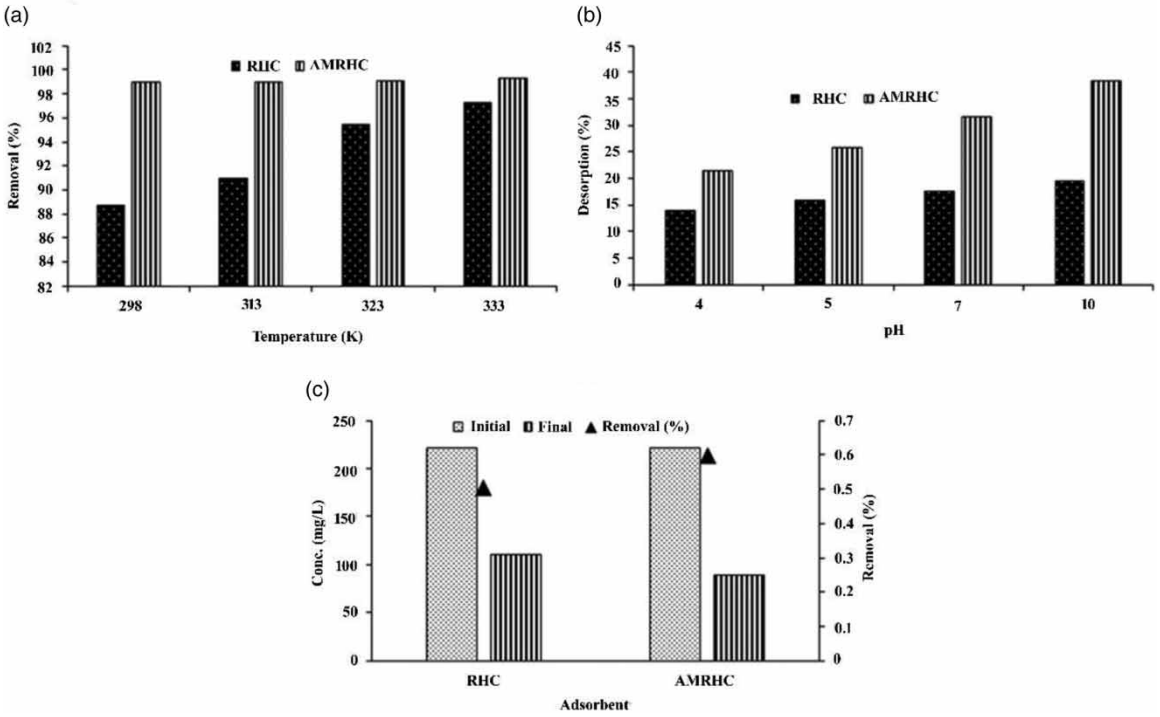

Figure 8 | (a) Effect of temperature on removal of MO by RHC and AMRHC, (b) desorption of MO by RHC and AMRHC, and (c) proportional MO removal from industrial wastewater.

occurs between MO molecules and RHC and AMRHC, respectively. Chakraborty *et al.* (2021) also found similar types of results where they suggesting that strong and weak binding forces may have existed between the adsorbent (Mahagoni wood charcoal and Mahagoni bark charcoal) and the reactive red 120.

MO removal from industrial wastewater by RHC and AMRHC

The efficiency of RHC and AMRHC for MO removal from industrial wastewater was assessed using the optimized adsorption experimental conditions. A textile effluent sample was collected from an industrial area in Saver, Dhaka, Bangladesh. Before the experiment, the pH (8.3), EC (731 μS/cm), TDS (353 mg/L), salinity (0.3 g/L), and MO concentration (221.28 mg/L) of the wastewater were determined. Figure 8(c) shows the proportional MO removal using the two adsorbents. The studies were conducted at pH 3, volume of 150 mL, and adsorbent dose of 10 g/L. The mixture was separated by filtration after stirring for 150 min for RHC and 120 min for AMRHC. The agitation speed was 180 rpm. Proportional MO removal was 50% for RHC and 60% for AMRHC, indicating that both adsorbents are appropriate for MO removal from polluted water.

CONCLUSIONS

This study focuses on MO removal from aqueous solutions and wastewater using RHC and AMRHC. The optimal pH (3) gave maximum MO adsorption for both adsorbents. The maximum adsorption capacities of the adsorbents were 4.57 and 11.53 mg/g, respectively. The Freundlich and Langmuir isotherms gave the best-fits with the experimental data for RHC and AMRHC, respectively. The kinetic investigation showed that the pseudo-second-order kinetic model gave the better fit with a multi-step diffusion process. The FTIR analysis indicates that –OH group and heteroatoms are responsible for adsorption where SEM analysis also shows lots of active adsorption sites influences this adsorption. A thermodynamic study showed that the RHC and AMRHC adsorption processes are endothermic and favorable. It is concluded that both RHC and AMRHC could be effective in MO removal from aqueous solutions and wastewater because of their availability, low cost, adsorption capacity, and good kinetics.

ACKNOWLEDGEMENTS

We would like to thank the Department of Environmental Science and Technology, Jashore University of Science and Technology, Bangladesh, for providing the necessary support.

FUNDING

The authors would like to thank the Ministry of Science and Technology, Bangladesh, for the research grant (R&D) award.

DATA AVAILABILITY STATEMENT

All relevant data are included in the paper or its Supplementary Information.

CONFLICT OF INTEREST

The authors declare there is no conflict.

REFERENCES

Alardhi, S. M., Fiyadh, S. S., Salman, A. D. & Adelikhah, M. 2023 Prediction of methyl orange dye (MO) adsorption using activated carbon with an artificial neural network optimization modeling. *Heliyon* e12888. https://doi.org/10.1016/j.heliyon.2023.e12888.

Arumugam, T. K., Krishnamoorthy, P., Tamilarasan, R. & Rajagopalan, N. R. 2018 Efficient usage of rice husk carbon and chitosan composite for adsorption of rhodamine B from wastewater. *Journal of Pharmaceutical, Chemical and Biological Sciences* **6**, 107–121.

Bensalah, H., Younssi, S. A., Ouammou, M., Gurlo, A. & Bekheet, M. F. 2020 Azo dye adsorption on an industrial waste-transformed hydroxyapatite adsorbent: kinetics, isotherms, mechanism and regeneration studies. *Journal of Environmental Chemical Engineering* **8**(3), 103807. https://doi.org/10.1016/j.jece.2020.103807.

Carolin, C. F., Kumar, P. S. & Joshiba, G. J. 2021 Sustainable approach to decolourize methyl orange dye from aqueous solution using novel bacterial strain and its metabolites characterization. *Clean Technologies and Environmental Policy* **23**(1), 173–181. https://doi.org/10.1007/s10098-020-01934-8.

Chakraborty, T. K., Islam, M. S., Zaman, S., Kabir, A. H. M. E. & Ghosh, G. C. 2020 Jute (*Corchorus olitorius*) stick charcoal as a low-cost adsorbent for the removal of methylene blue dye from aqueous solution. *SN Applied Sciences* **2**(4), 765. https://doi.org/10.1007/s42452-020-2565-y.

Chakraborty, T. K., Ghosh, G. C., Akter, M., Adhikary, K., Islam, M., Ghosh, P., Zaman, S., Habib, A. & Kabir, A. H. M. 2021 Biosorption of reactive red 120 dye from aqueous solutions by using Mahagoni (*Swietenia mahagoni*) wood and bark charcoal: equilibrium, and kinetic studies. *Pollution* **7**(4), 905–921. https://doi.org/10.22059/poll.2021.325135.1110.

Fu, Y., Shen, Y., Zhang, Z., Ge, X. & Chen, M. 2019 Activated bio-chars derived from rice husk via one-and two-step KOH-catalyzed pyrolysis for phenol adsorption. *Science of the Total Environment* **646**, 1567–1577. https://doi.org/10.1016/j.scitotenv.2018.07.423.

Ghosh, G. C., Samina, Z. & Chakraborty, T. K. 2018 Adsorptive removal of Cr (VI) from aqueous solution using rice husk and rice husk ash. *Desalination and Water Treatment* **130**, 151–160. https://dx.doi.org/10.5004/dwt.2018.22828.

Ghosh, G. C., Chakraborty, T. K., Zaman, S., Nahar, M. N. & Kabir, A. H. M. E. 2020 Removal of methyl orange dye from aqueous solution by a low-cost activated carbon prepared from Mahagoni (*Swietenia mahagoni*) bark. *Pollution* **6**(1), 171–184. https://dx.doi.org/10.22059/poll.2019.289061.679.

Huang, R., Liu, Q., Huo, J. & Yang, B. 2017 Adsorption of methyl orange onto protonated cross-linked chitosan. *Arabian Journal of Chemistry* **10**(1), 24–32. https://doi.org/10.1016/j.arabjc.2013.05.017.

Kubendiran, H., Hui, D., Pulimi, M., Chandrasekaran, N., Murthy, P. S. & Mukherjee, A. 2021 Removal of methyl orange from aqueous solution using SRB supported bio-Pd/Fe NPs. *Environmental Nanotechnology, Monitoring & Management* **16**, 100561. https://doi.org/10.1016/j.enmm.2021.100561.

Lafi, R. & Hafiane, A. 2016 Removal of methyl orange (MO) from aqueous solution using cationic surfactants modified coffee waste (MCWs). *Journal of the Taiwan Institute of Chemical Engineers* **58**, 424–433. https://doi.org/10.1016/j.jtice.2015.06.035.

Leng, L., Yuan, X., Zeng, G., Shao, J., Chen, X., Wu, Z., Wang, H. & Peng, X. 2015 Surface characterization of rice husk bio-char produced by liquefaction and application for cationic dye (Malachite green) adsorption. *Fuel* **155**, 77–85. https://doi.org/10.1016/j.fuel.2015.04.019.

Palapa, N. R., Taher, T., Rahayu, B. R., Mohadi, R., Rachmat, A. & Lesbani, A. 2020 CuAl LDH/rice husk biochar composite for enhanced adsorptive removal of cationic dye from aqueous solution. *Bulletin of Chemical Reaction Engineering & Catalysis* **15**(2), 525–537. https://doi.org/10.9767/bcrec.15.2.7828.525-537.

Radoor, S., Karayil, J., Jayakumar, A., Parameswaranpillai, J. & Siengchin, S. 2021 Efficient removal of methyl orange from aqueous solution using mesoporous ZSM-5 zeolite: synthesis, kinetics and isotherm studies. *Colloids and Surfaces A: Physicochemical and Engineering Aspects* **611**, 125852. https://doi.org/10.1016/j.colsurfa.2020.125852.

Umpuch, C. & Sakaew, S. 2013 Removal of methyl orange from aqueous solutions by adsorption using chitosan intercalated montmorillonite. *Songklanakarin Journal of Science & Technology* **35**(4), 451–459.

Yönten, V., Sanyürek, N. K. & Kivanç, M. R. 2020 A thermodynamic and kinetic approach to adsorption of methyl orange from aqueous solution using a low cost activated carbon prepared from *Vitis vinifera* L. *Surfaces and Interfaces* **20**, 100529. https://doi.org/10.1016/j.surfin.2020.100529.

Zaman, S., Mehrab, M. N., Islam, M. S., Ghosh, G. C. & Chakraborty, T. K. 2021 Hen feather: a bio-waste material for adsorptive removal of methyl red dye from aqueous solutions. *H2Open Journal* **4**(1), 291–301. https://doi.org/10.2166/h2oj.2021.123.

Zaman, S., Biswas, P., Zaman, R., Islam, M. S., Mehrab, M. N., Ghosh, G. C., Habib, A. & Chakraborty, T. K. 2022 Jute (*Corchorus olitorius*) stick charcoal: a potential bioadsorbent for the removal of Cr (VI) from an aqueous solution. *H2Open Journal* **5**(4), 656–669. https://doi.org/10.2166/h2oj.2022.027.

First received 21 June 2023; accepted in revised form 2 August 2023. Available online 17 August 2023